HYDROLOGICAL PROCESSES
Hydrol. Process. **21**, 1997–2008 (2007)
Published online in Wiley InterScience
(www.interscience.wiley.com) DOI: 10.1002/hyp.6706

Surface flux and atmospheric boundary layer observations from the LAPS project over the middle stream of the Huaihe River basin in China

Hiroki Tanaka,[1,2,3]* Tetsuya Hiyama,[1] Koh Yamamoto,[3] Hatsuki Fujinami,[1] Taro Shinoda,[1] Atsushi Higuchi,[4] Satoshi Endo,[3] Shoichiro Ikeda,[5] Weijing Li[6] and Kenji Nakamura[1]

[1] *Hydrospheric Atmospheric Research Center, Nagoya University, Nagoya 464-8601, Japan*
[2] *Core Research for Evolutional Science and Technology, Japan Science and Technology Corporation, Kawaguchi 332-0012, Japan*
[3] *Graduate School of Environmental Studies, Nagoya University, Nagoya 464-8601, Japan*
[4] *Center for Environmental Remote Sensing, Chiba University, Chiba 263-8522, Japan*
[5] *Graduate School of Natural Science and Technology, Okayama University, Okayama 700-8530, Japan*
[6] *National Climate Center, Chinese Meteorological Administration, Beijing 100081, China*

Abstract:

Observations of the surface layer and the atmospheric boundary layer (ABL) were collected as part of the Lower Atmosphere and Precipitation Study (LAPS), which investigated the relationship between the surface conditions and the ABL processes. The LAPS was part of the Core Research for Evolutional Science and Technology (CREST) program, under the auspices of the Japan Science and Technology Agency (JST). Observations began in August 2003 over a flat surface region in mid-latitude China at 32·55 °N, 116·78 °E. Observations before, during, and after the Meiyu season in China provided data for surface conditions varying from relatively dry to moist. Preliminary analysis of the surface and the ABL observations shows relationships between the surface fluxes and the ABL structure. ABL depth was enhanced by sensible heat flux. Fluctuations in the ABL depth corresponded to plume-like wind structures within the ABL. Day-to-day variability in ABL depth was controlled mainly by buoyancy flux over the surface during dry periods. It was also affected by vertical motion at the top of the ABL, especially during wet periods. Copyright © 2007 John Wiley & Sons, Ltd.

KEY WORDS surface heat flux; atmospheric boundary layer; wind profiler radar; Meiyu in China

Received 29 June 2005; Accepted 1 February 2006

INTRODUCTION

Interactions between the surface and the atmospheric boundary layer (ABL) at various temporal and spatial scales are an important research topic in air pollution studies, hydrology, meteorology, and climatology. Surface conditions, including soil moisture and vegetation cover, affect the ABL structure, cloudiness, and precipitation (Wai and Smith, 1998). Simultaneous observations of surface and ABL processes under various surface conditions are required to understand the interactions involved. Wind profiler radar (WPR) recorded ABL measurements concurrently with flux measurements above the surface in the First International Satellite Land Surface Climatology Project (ISLSCP) Field Experiment (FIFE) (Sellers *et al*., 1992) in 1989. Wai and Smith (1998) showed that soil moisture affected the ABL development. Furthermore, biophysically induced ABL forcing, associated with a gradient in organized vegetation cover, can sustain mesoscale circulations within a $\sim$16 km^2 domain. Angevine *et al*. (1998) reported the preliminary results of the simultaneous observations of WPR and surface flux from the Flatland Project in 1996, and described the diurnal and seasonal variations in the ABL depth and the surface flux for flat terrain in Illinois, USA.

Simultaneous observations of the WPR and the surface flux measurements have not yet been reported for the Asian monsoon region, although many individual surface or ABL observations have been recorded under the Global Energy and Water Cycle Experiment (GEWEX) Asian Monsoon Experiment (GAME) and GAME-related projects (e.g. Hiyama *et al*., 1999, 2003; Ohta *et al*., 1999, 2001; Sugita *et al*., 1999; Asanuma *et al*., 2000; Reddy *et al*., 2001; Tanaka *et al*., 2001; Toda *et al*., 2002; Komatsu *et al*., 2003; Choi *et al*., 2004; Gao *et al*., 2004; Strunin *et al*., 2004; Strunin and Hiyama, 2004; Gao, 2005; Shinoda *et al*., 2005). The simultaneous observations reported here will fill this gap. The Asian monsoon over Far East Asia has unique characteristics, such as the Meiyu frontal activity that persists during the summer rainy season in this region and plays an important role in the regional climate as well as the global climate. The Lower Atmosphere and Precipitation Study (LAPS) is a post-GAME project sponsored by the Core Research for Evolutional Science and Technology (CREST) program of the Japan Science and Technology Agency (JST). This program seeks to clarify precipitation

* Correspondence to: Hiroki Tanaka, Graduate School of Environmental Studies, Nagoya University, Nagoya 464-8601, Japan.
E-mail: hiroki@hyarc.nagoya-u.ac.jp

onset mechanisms, including the relationships between the surface, ABL, clouds, and precipitation processes. Changes in surface conditions alter the surface heat and the water vapour fluxes that in turn affect the ABL structures. ABL processes are one of many triggers that generate clouds and precipitation. The ABL is the interface between the surface and the free atmosphere, and it strongly influences the vapour transport, sensible heat flux over the surface and convective precipitation systems. Clarifying ABL development mechanisms on diurnal and seasonal time scales will help elucidate regional hydrological budgets.

ABL depth, or the height of the top of the daytime convective mixed layer is an important parameter in the studies of the ABL. WPR is a kind of Doppler radar, which detects the atmospheric echo and its Doppler shifts due to the wind. Due to the Bragg scattering, the turbulence structure with the scale of half radar wavelength ($\lambda/2 \approx 0{\cdot}12$ m in this study) enhances to reflect the WPR beam. WPR detects the ABL top, as the level with maximum radar scattering or WPR echo, because the entrainment layer has large scalar gradients and therefore many turbulent structures (Angevine *et al*., 1994, 2001; Hashiguchi *et al*., 1995; White *et al*., 2002). The WPR echo intensity, or backscattered power, P_R, is given by the radar equation as

$$P_R = P_r \frac{\eta G^2 \lambda^2 \theta^2 h}{1024\pi^2 \ln 2 r^2} \quad (1)$$

where P_r is the transmitted peak power, G is the antenna gain, λ is the radar wavelength, r is the range to the backscatter volume, θ is the beam width, h is the pulse length, and η is the radar reflectivity per unit volume, which is proportional to the refractive index structure parameter C_n^2 as follows:

$$\eta = 0{\cdot}38 C_n^2 \lambda^{-1/3} \quad (2)$$

The structure parameter C_n^2 represents the intensity of turbulence, and strongly depends on gradients of vapour density.

Tennekes (1973) used conservation of virtual temperature within the ABL to estimate the ABL depth from the accumulated surface virtual temperature flux and the vertical motion at the top of the ABL. If vertical motion at the top of the ABL and horizontal advection are both negligible, ABL depth is related to surface heat flux as follows (cf., Garratt, 1992):

$$(z_0 + \Delta z)^2 = z_0^2 + \frac{2}{\Gamma}(1 + 2\varepsilon) Q_S \quad (3)$$

Here z_0 is the initial depth of the ABL, Δz is the increment of the depth for a reference duration, Γ is the lapse rate of potential temperature above the ABL, ε is an entrainment parameter, and Q_S is the surface virtual temperature flux that accumulated during the reference duration.

The main target of observations in this study was the surface-ABL relationship before, during, and after the Meiyu season in China. One goal was to understand how the drastic change in surface moisture conditions during the Meiyu season affects the ABL structure through surface flux interactions. The monitoring site is located in a transition area between humid and dry regions in China. The land surface in this vicinity is suddenly moistened during the Meiyu. Humidity persists in the lower atmosphere during the Meiyu season even when the Meiyu front temporarily moves south of the region. Thus, another goal was to describe the vapour source that provides or maintains such high humidity throughout the season. The presence of high humidity allows relatively small triggers to generate clouds and precipitation. Synoptic-scale water vapour transport and human activities, such as agricultural irrigation and cultivation, can influence the ABL moisture conditions through surface-ABL interactions. Surface and ABL monitoring in this flat region before, during, and after the Meiyu will provide important data.

This paper describes the surface and ABL observations in the LAPS project over the middle stream of the Huaihe River basin in China. Then, initial data from tower observations, WPR observations, and vegetation research are presented. Finally, relationships are presented between the ABL depth and the surface heat fluxes and other parameters, such as the vertical motion at the top of the ABL.

MATERIALS AND METHODS

Site description

The study site was a flat surface region located in Shouxian, China, at 32·55 °N and 116·78 °E, 22·7 m A.S.L. The site is located near the Huaihe River in Anhui Province, China (Figure 1). Instrumentation at the study site included an ABL wind profiler radar (L-28, Sumitomo Electric Industries, Ltd, Japan), an acoustic wind profiler SODAR (XFAS, Scintec, A.G., Germany), a microwave water vapour profiler (TP/WVP-3000, Radiometrics, Co., USA), and a surface-layer observation system (C-PRJ30 and C-FLJ30, Climatec, Inc., Japan) at the Shouxian Meteorological Observatory, Anhui Meteorological Bureau, Chinese Meteorological Administration. The site is located at the southern edge of residential Shouxian, 2 km south of the city center. Surrounding land are mainly agricultural fields, with some residences and small buildings that are often surrounded by trees. A paved road passes 200 m west of the site, and there is an irrigation canal 2 km west of the road. Lake Wabuhu is 7 km southeast of the site, and the Huaihe River passes 9 km northwest.

Monitoring for the LAPS project started in August 2003 and is ongoing, although interruptions occurred because of power supply problems, instruments affected by strong wind or lightning, and other problems. Intensive observations, including vegetation research, were recorded during the intensive observation period (IOP) from 24 May to 16 July in 2004 (IOP-2004). Land use

DOI: 10.1002/hyp

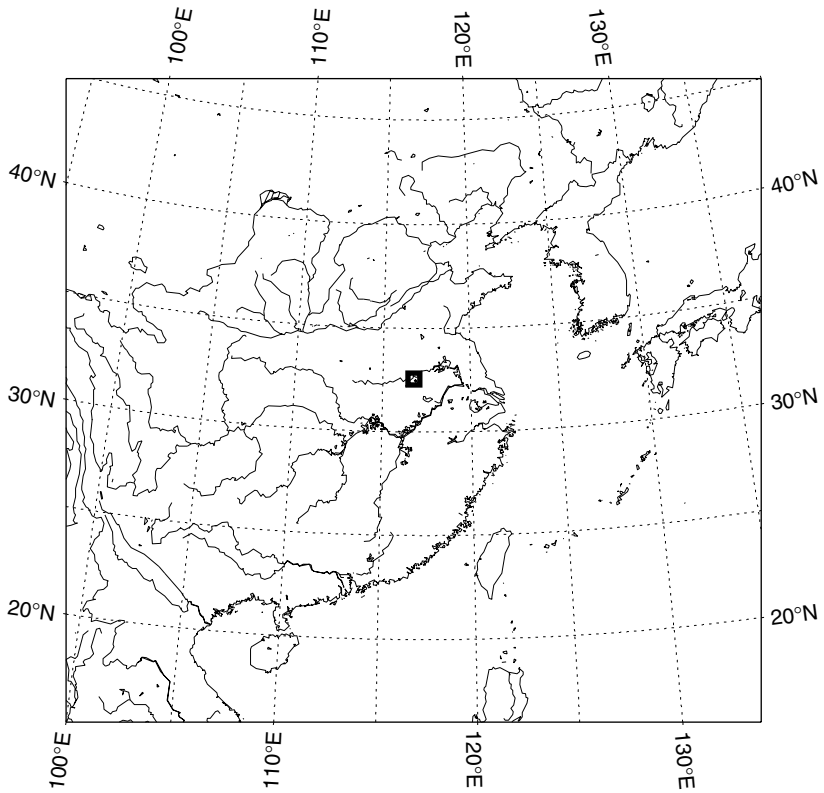

Figure 1. Location of the study site, Shouxian, at 32·55 °N, 116·78 °E, and 22·7 m A.S.L., near the Huaihe River in Anhui Province, China. The study site is indicated as the marker (■)

Table I. Variables observed during the intensive observation period from 24 May to16 July 2004 (IOP-2004) in the Lower Atmosphere and Precipitation Study (LAPS)

Variables	Intervals	Notes
Water temperature	1 h during daytime, 08 : 00–17 : 00 LT	No water before 14 JUNE
Soil temperature	1 h during daytime, 08 : 00–17 : 00 LT	At 0·1 m below-ground
Surface temperature	1 h during daytime, 08 : 00–17 : 00 LT	Soil surface before 14 JUNE; Water surface after 15 JUN
Vegetation height	Once per day	No vegetation between 31 MAY and 15 JUNE
Water depth	Once per day	No water before 14 JUNE
SPAD[a]	Once per day	No vegetation between 31 MAY and 15 JUNE
Leaf area index (LAI)	5 times, 25 MAY, 16 JUNE, 24 JUNE, 30 JUNE, 7 JULY	No vegetation between 31 MAY and 15 JUNE
Cloud amount	Twice per day	Using fish-eye sky photos and weather condition records

[a] An index of the chlorophyll density obtained by a chlorophyll sensor (SPAD-502, Konica Minolta, Japan).

surrounding the site changed from wheat field to rice paddy field during IOP-2004.

Observation items

IOP-2004 included observations of vegetation cover surrounding the study site. Table I summarizes parameters observed manually at the study site. Surface-layer variables include turbulent fluxes, radiation fluxes, wind speed, wind direction, air temperature, atmospheric humidity, soil temperature, soil moisture, and precipitation rate. These were all measured with a surface-layer observation system on a 32·2-m tower and two 3·5-m masts. Table II summarizes the observed items and individual instruments within the system. The turbulent fluxes obtained at the height of 32·0 m were used for analyses in this study, because the dependency on the wind direction was less detected than those obtained at other lower levels.

ABL parameters, including wind vectors and a turbulence structure parameter, were measured using a 1·29-GHz WPR. Table III summarizes the WPR operational specifications. The maximum height of the observation was approximately 8000 m. The resolution of the observed wind velocities was 0·1 ms^{-1} (horizontal) and 0·01 ms^{-1} (vertical). The accuracy was less than 1 ms^{-1} in horizontal and less than 0·1 ms^{-1} in vertical. The observation range was 0–90 ms^{-1} (horizontal) and 0–30 ms^{-1} (vertical). The original WPR data have

DOI: 10.1002/hyp

Table II. Observed variables and instruments for the surface layer observation system

Variables	Instruments	Height or depth (m)
Wind vector and virtual temperature	C-SAT-R3-50 (1210R3), Gill	32·0, 12·2, 3·5
CO_2 and H_2O density	C-CS7500 (LI-7500), Li-Cor	32·0, 12·2, 3·5
Atmospheric pressure	CVS-PTB210, Vaisala	2·5
Wind velocity	C-PR-010C, MetOne	32·2, 21·9, 11·9, 3·0, 1·6
Wind direction	C-PR-020C, MetOne	31·8
Radiation fluxes (four components)	C-PR-CNR1, Kip & Zonen	31·8
Air temperature and humidity	C-PR-45D (HMP-45D), Vaisala	30·7, 20·7, 10·8, 2·8, 1·5
Surface temperature	C-303F	30·7, 2·9
Soil moisture content	C-CS616-30, Campbell	−0·1, −0·2, −0·4
Ground heat flux	C-PRHF01, Huxflux	−0·01, −0·01, −0·01
Ground soil temperature	C-PT100	−0·05, −0·1, −0·2, −0·4, −0·4
Precipitation	COT-34T, Ota Keiki	0
Water level	Floating gauge	0

Table III. Operation specifications for the wind profiler radar

Variables	Values
Radar operational frequency	1290 MHz
Pulse length	666 ns
Sampling interval	666 ns
Inter-pulse period	80000 ns
Number of height points	80
Number of coherent integrations	32
Number of FFT points	128
Number of incoherent integrations	18
Number of beam directions	5
Direction of beam (azimuth, zenith) (deg)	(0, 0), (0, 15), (90,15), (180, 15), (270, 15)

a time interval of about 59 s, and a height resolution of 99·9 m for vertical beams and 96·4 m for oblique beams.

For ease data inspection, data in this study were gridded with two-dimensional interpolation as;

$$X(t,h) = \sum_{D^2<1.5} \frac{x(t_r,h_r)}{D^2} \Big/ \sum_{D^2<1.5} \frac{1}{D^2} \tag{4}$$

where $X(t, h)$ is the interpolated value at time t (s) and height h (m), $x(t_r, h_r)$ is the original data at time t_r (s) and height h_r (m), and D^2 is the square of the dimensionless distance defined as follow;

$$D^2 = \left(\frac{h-h_r}{100}\right)^2 + \left(\frac{t-t_r}{60}\right)^2 \tag{5}$$

The time interval of the gridded data is 30 s, and the height resolution is 50 m.

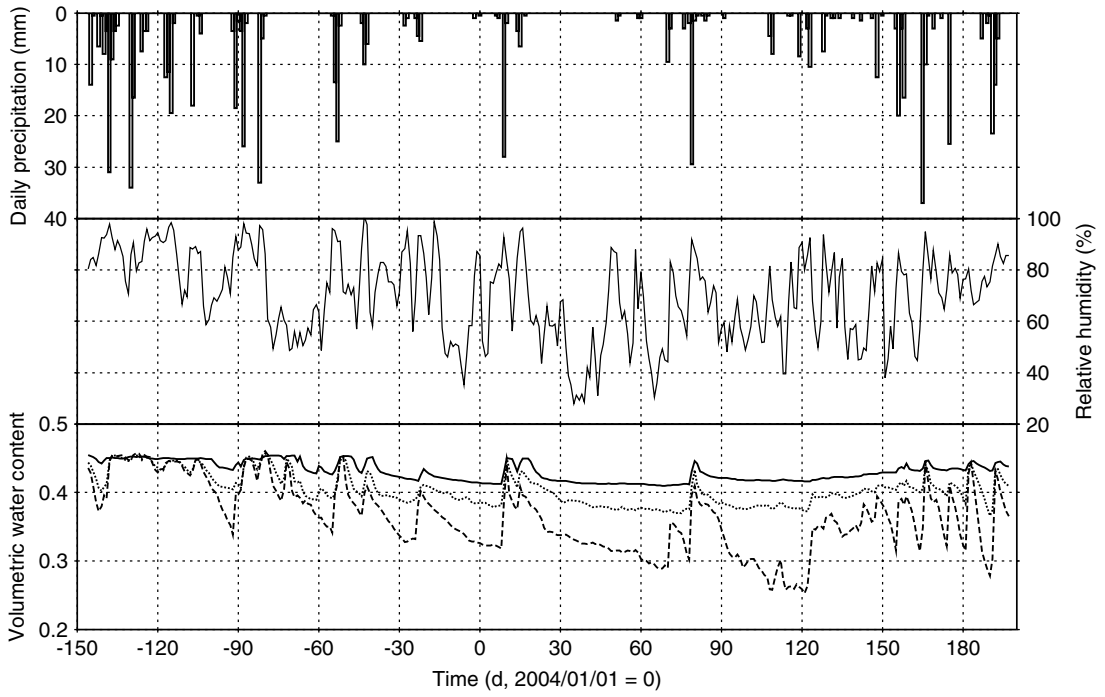

Figure 2. Seasonal variation of the daily precipitation (upper column), daily relative humidity (middle column), and volumetric soil water content (bottom column) at 0·4 m depth (solid), 0·2 m depth (dots), and 0·1 m depth (dashes) in non-irrigated ground near the flux tower for approximately 1 year, from 8 August 2003 to 16 July 2004

DOI: 10.1002/hyp

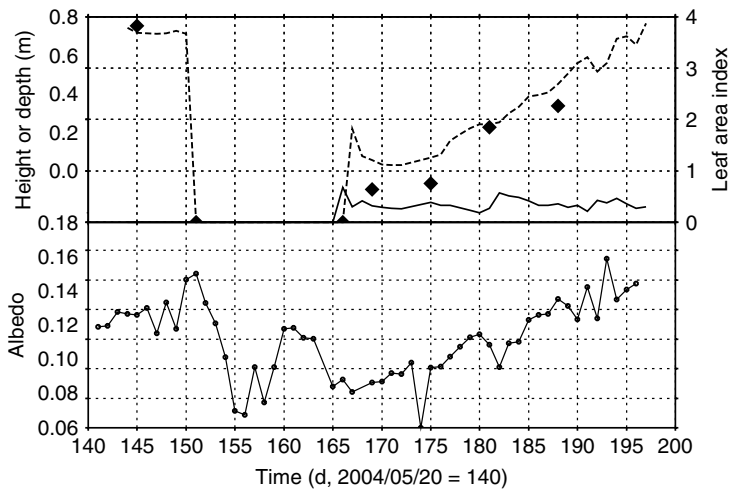

Figure 3. Changes in plant height (dashed line, left axis), leaf area index (rectangle, right axis), irrigated water depth (solid line, left axis), and albedo (solid line with circles) during IOP-2004

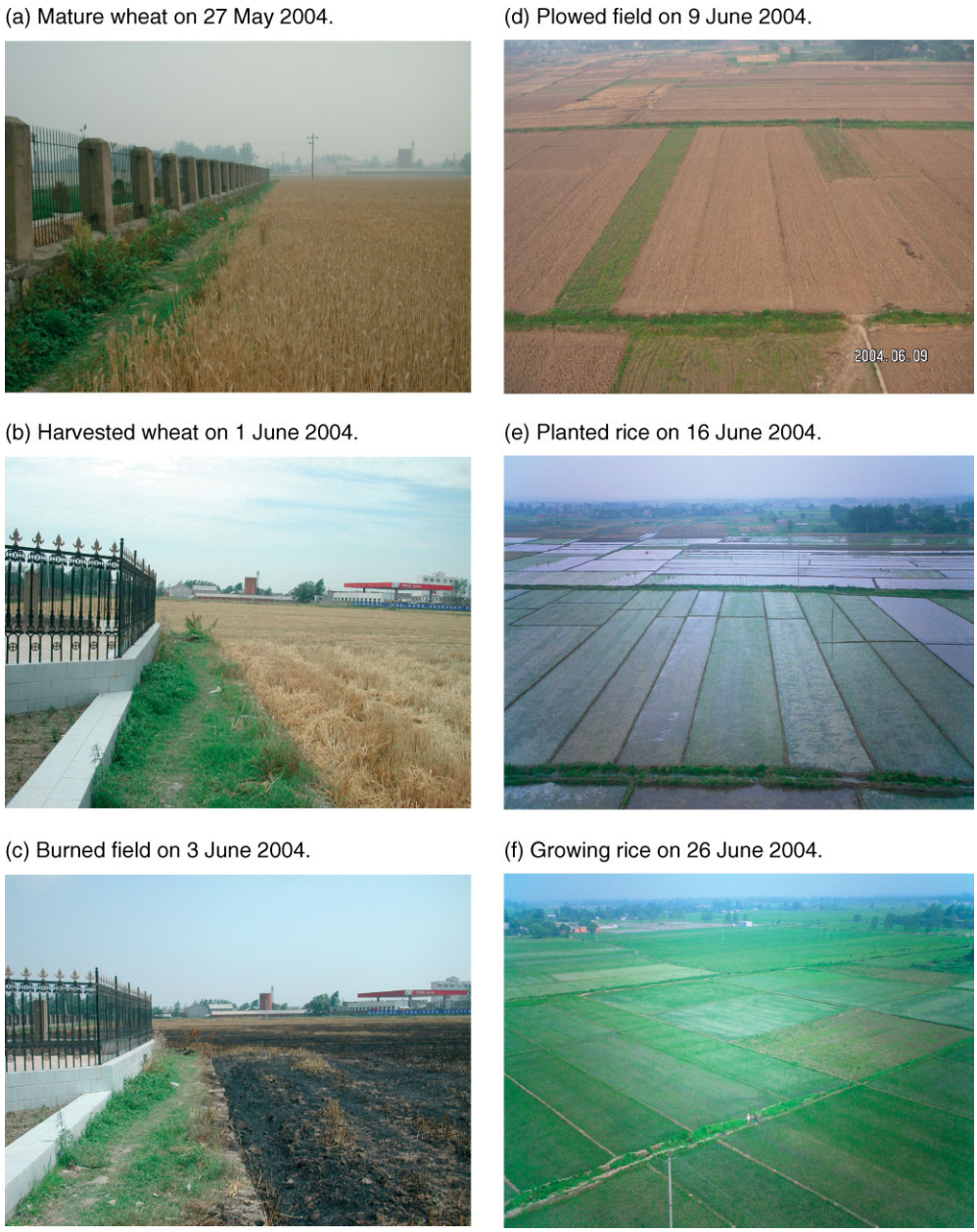

Figure 4. Land-use photographs. (a) Mature wheat on 27 May 2004, (b) harvested wheat on 1 June 2004, (c) burned field on 3 June 2004, (d) plowed field on 9 June 2004, (e) planted rice on 16 June 2004, (f) growing rice on 26 June 2004

DOI: 10.1002/hyp

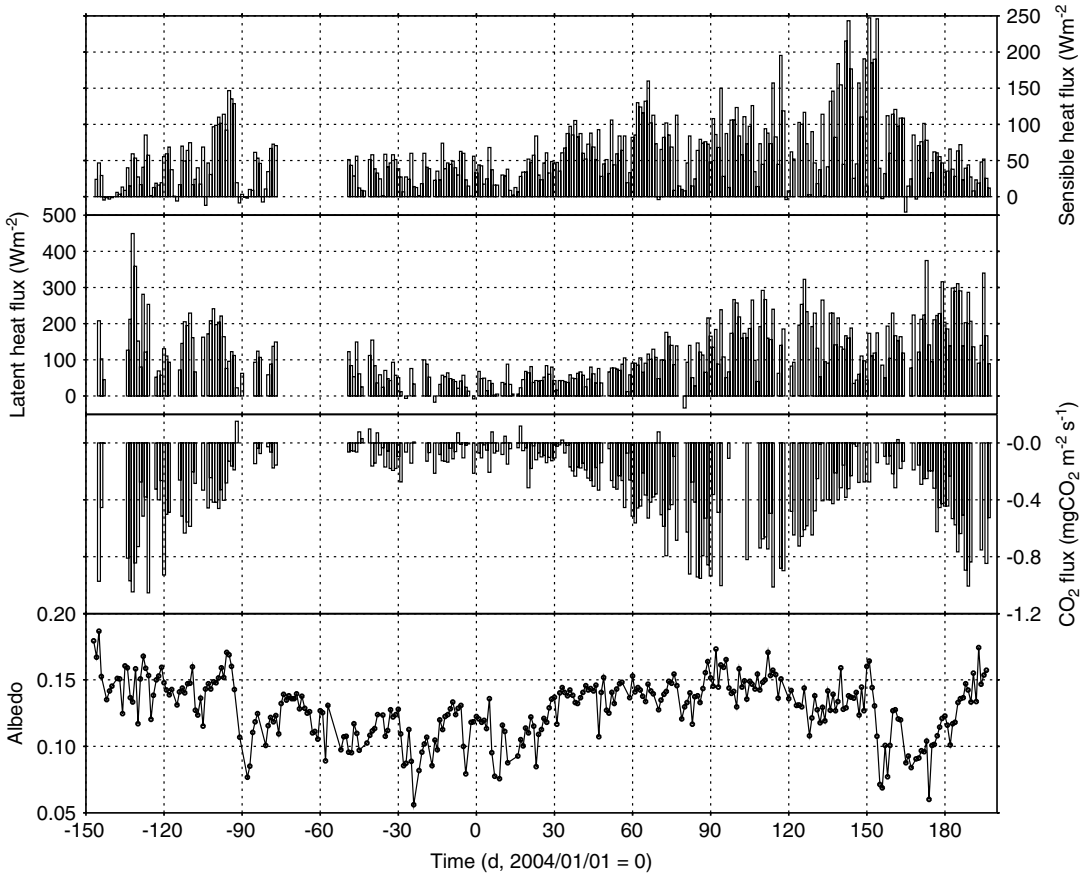

Figure 5. Seasonal variation of midday virtual sensible heat, latent heat, and CO_2 flux averaged between 08 : 00 and 16 : 00 LT, and short-wave albedo averaged between 11 : 00 and 13 : 00 LT

Estimation of the ABL depth from WPR data

The ABL depth can be estimated theoretically or empirically, as the height with the maximum echo intensity received by the WPR. Angevine *et al*. (1994) proposed the so-called 'median filtering method' to estimate the ABL depth as the median value of the maximum echo heights for certain durations (e.g. 30 min). However, such estimates sometimes fail because of large returns from clouds above the ABL or from strong near-surface turbulence. Such failures can be avoided by estimating the ABL depth over much longer time periods (e.g. more than 2–4 h), or by limiting the height range in which the ABL top can appear. The latter method allows fluctuations within a short time scale and was chosen for this study. Assumptions that limited the possible height range were: the convective mixed layer started to develop just after sunrise, around 06 : 00 local time (LT); the peak height appeared between 12 : 00 and 16 : 00 LT; the height remained within approximately the same range after 16 : 00 LT. This diurnal evolution of the ABL height was usually valid for days without significant clouds or precipitation.

RESULTS AND DISCUSSION

Overview of the climate and surface conditions

Figure 2 shows seasonal changes in the volumetric soil water content of the non-irrigated ground near the tower, the relative humidity on the tower, and the daily precipitation from 8 August 2003 to 16 July 2004. Soil water content increased following precipitation events. Atmospheric humidity was high during the summer. Soils were generally moist (the soil porosity was approximately 0·45) during the entire year, except near the surface during some dry spells in winter and early spring.

Figure 3 shows plant height, leaf area index (LAI), irrigated water depth, and albedo (α) during IOP-2004. A land-use change is illustrated by the photographs in Figure 4. Mature wheat ($\alpha \sim 0{\cdot}14$) was the dominant vegetation between 24 May (time = 144 in Figure 3) and 30 May (time = 150), at which time it was harvested ($\alpha \sim$ 0·16). Wheat litter was burned ($\alpha \sim 0{\cdot}07$) between 1 June and 4 June (time = 152–155). The black ash was plowed down ($\alpha \sim 0{\cdot}12$), and rice seedlings were planted and flooded ($\alpha \sim 0{\cdot}09$) on 14 June (time = 165). The planted seedlings were 0·2–0·3 m tall. The seedlings grew to 0·7–0·8 m ($\alpha \sim 0{\cdot}15$) on 16 July (time = 197), the end of IOP-2004.

Water vapour was transported by synoptic-scale southerly winds on 14 June (time = 165), when irrigation started. After this day, moisture persisted in the lower atmosphere (Figure 2), even when drier air blow in from the north, i.e. when the Meiyu front moved south. The sudden increase in atmospheric moisture may have been driven by synoptic-scale moisture transport, and partly by irrigation. Maintenance of high humidity within the

DOI: 10.1002/hyp

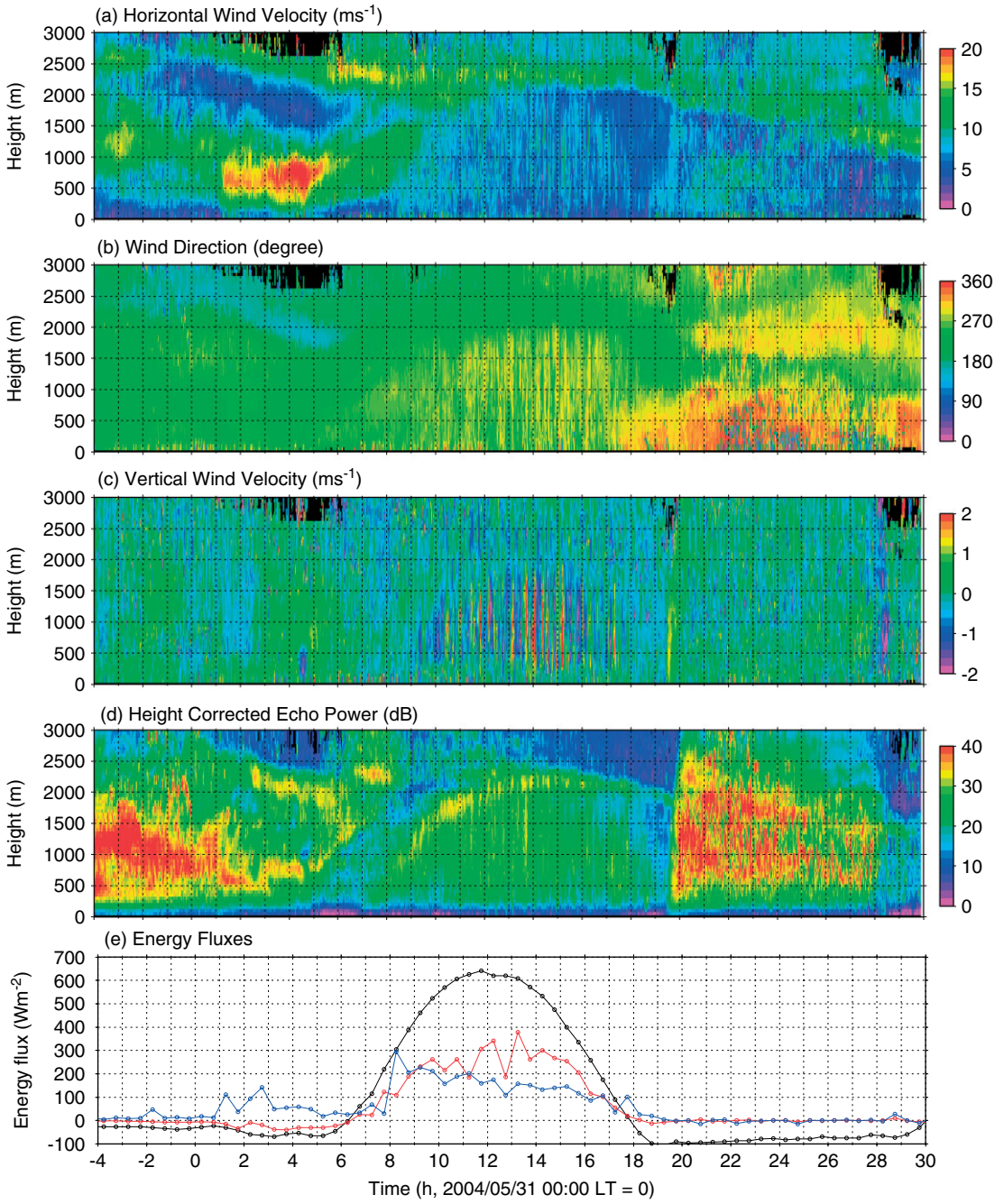

Figure 6. Typical diurnal changes in the ABL structure and the surface flux in on 31 May 2004 when vegetation cover is not present. (a) Horizontal wind speed, (b) wind direction, (c) vertical wind velocity, (d) echo intensity, and (e) energy fluxes including net radiation (black), virtual sensible heat flux (red), and latent heat flux (blue)

ABL resulted likely from the surface water during the wet season.

Figure 5 shows the seasonal changes in midday virtual sensible and latent heat fluxes and CO_2 flux averaged between 08 : 00 and 16 : 00 LT, and the short-wave albedo averaged between 11 : 00 and 13 : 00 LT. Virtual sensible heat flux, rather than the sensible heat flux, is shown in Figure 5 and subsequent figures to account more clearly for buoyancy effects. The two fluxes differ by approximately 6 Wm^{-2} when the latent heat flux is 100 Wm^{-2}. Virtual sensible heat flux H_v is defined as:

$$H_V = H + 0{\cdot}514 C_P T_V E \quad (6)$$

where C_P is the specific heat of air, T_v is the virtual temperature, and E is the water vapour flux. Changes in land-use clearly affect the parameters. Rice fields were present during summer, and high rates of CO_2 absorption and evapotranspiration, and small values of sensible heat flux indicate growing rice during August 2003. Mature rice is indicated in September 2003 by decreased CO_2 absorption and evapotranspiration and increased sensible heat flux. Low albedo and small fluxes accompany sparse vegetation from October through January 2004. As wheat germinated and grew between February and April, CO_2 absorption and evapotranspiration increased. Wheat

DOI: 10.1002/hyp

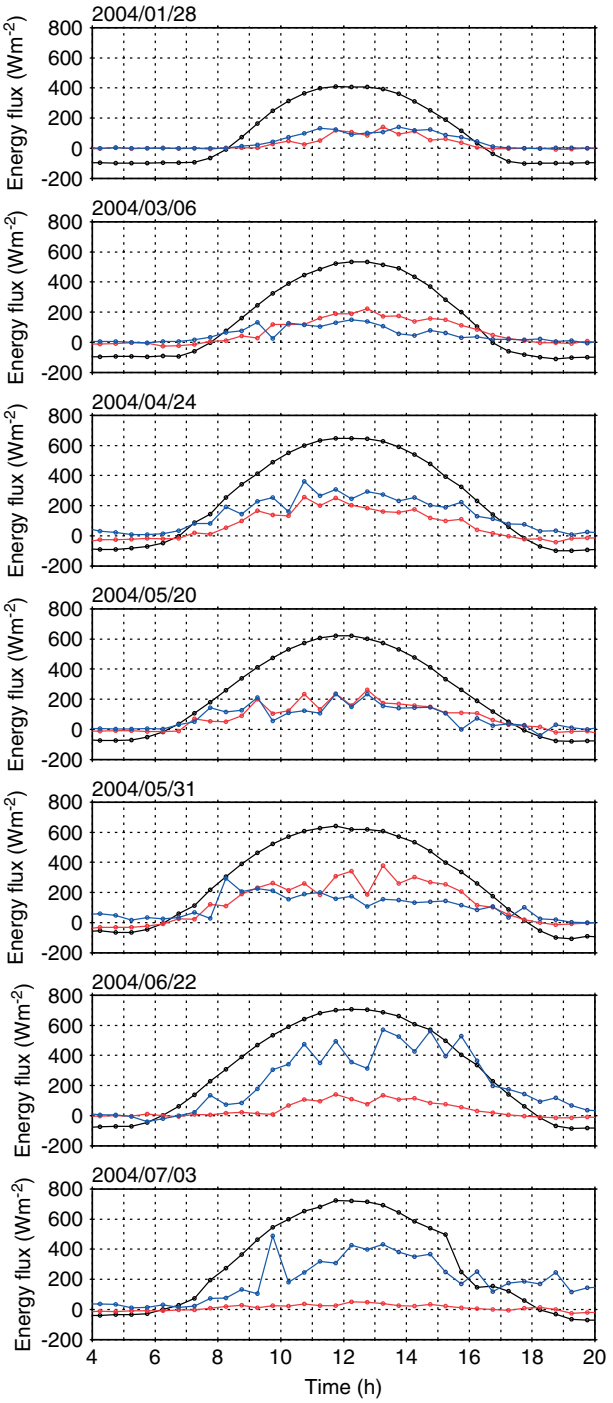

Figure 7. Diurnal changes in energy fluxes over the surface on 7 clear days: 28 January, 6 March, 24 April, 20 May, 31 May, 22 June, and 3 July. Black line indicates net radiation, red line indicates virtual sensible heat flux, and blue line indicates latent heat flux

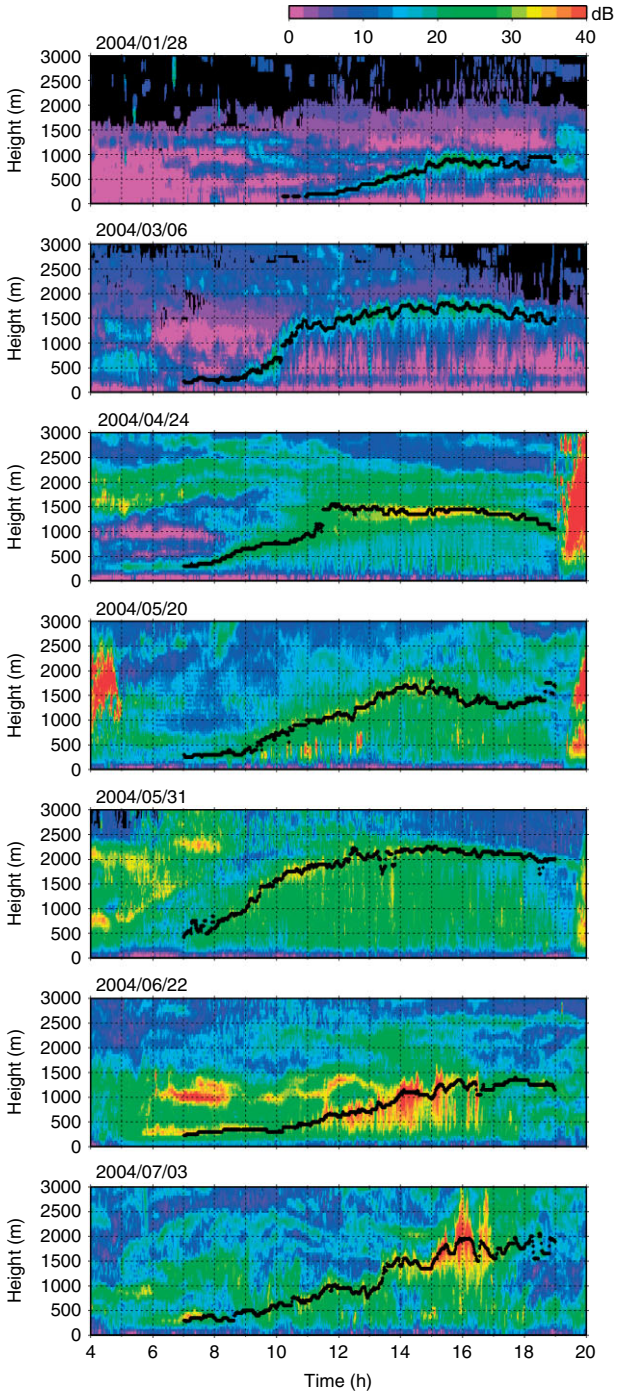

Figure 8. Time-height sections of echo intensity obtained from wind profiler radar observations on several typical days (same as in Figure 7). Atmospheric boundary layer depth was estimated every 2 min (black dots)

matured during May, when CO_2 absorption and vapour flux decreased, sensible heat flux was large, and albedo decreased slightly. Rice seedlings were planted again in mid-June 2004, and subsequently grew until mid-July as CO_2 absorption, water vapour flux, and albedo increased, and sensible heat flux decreased.

Diurnal development of the ABL depth

Figure 6 shows typical diurnal changes in ABL structure and surface fluxes when no vegetation cover existed on 31 May (time = 151 in Figure 2). The figure includes (a) horizontal wind speed, (b) wind direction, (c) vertical wind velocity, (d) echo intensity, and (e) net radiation, virtual sensible heat flux, and latent heat flux. Echo intensity (Figure 6d) depicts turbulence intensity, or the turbulence structure parameter C_n^2 (refer Equations 1 and 2). A convective mixed layer was present during the day and strong WPR echoes were detected. The ABL depth clearly increased from soon after sunrise till the afternoon. There were strong horizontal winds and sudden

DOI: 10.1002/hyp

changes in wind direction above the top of the ABL in daytime (cf., Figure 6(a) and (b)). The ABL depth fluctuated as echo intensity within the ABL varied, being periodically enhanced by plume-like structures in the upward wind (red in Figure 6(c)), which alternated with downward wind structures (blue in Figure 6(c)) between 09 : 00 and 17 : 00 LT. The period was 30–60 min on typical fine days. The plume-like upward wind extended to the top of the ABL at midday. Plumes did not reach the top of the ABL in late afternoon.

Much stronger echoes were often detected at night, especially just after sunset. Heights often exceeded 2500 m. Similar phenomena had been recognized in the past as contamination from migrating birds. Wilczak *et al*. (1995) considered possible reasons behind the appearance of strange echoes. Kobayashi *et al*. (2005) concluded that migrating birds can scatter the WPR beam, and proposed a method to eliminate this effect from observed wind velocity. However, no migrating birds were observed when the anomalous echoes were present in this study, and it seems unlikely that they would be present every night. The reason for these anomalous echoes will be the subject of future study. The following sections focus on ABL development during the day.

Seasonal changes in the ABL depth

Figure 7 shows the diurnal changes in energy fluxes over the surface on seven clear days. Wheat was sprouting around 28 January (time = 27 in Figure 2), growing on 6 March (time = 65) and 24 April (time = 114), mature on 20 May (time = 140), and harvested on 31 May (time = 151). Subsequently, rice was growing on 22 June (time = 173) and 3 July (time = 184). Virtual sensible heat flux is simply referred as sensible heat flux in the following sentences, because the two fluxes differ little (refer Equation 6). Sensible and latent heat fluxes had similar diurnal traces that tracked the diurnal changes in the net radiation before the wheat was harvested. When the wheat was most actively growing, the latent heat flux slightly exceeded the sensible heat flux (on 24 April). The latent heat flux decreased between wheat harvest and field flooding (31 May). Sensible heat flux dropped and the latent heat flux increased dramatically after the field was flooded and rice seedlings were planted (22 June and 3 July); the peak latent heat flux shifted later in the day because the high heat capacity of the irrigation water allowed higher temperatures to persist till the evening.

Figure 8 shows the echo intensities and the ABL depths, recorded by the WPR on the same days as in Figure 7. The ABL depth was derived every 2 min using the procedures outlined above. The ABL depth reached 1500 m around noon, before irrigation, except in winter: the ABL was less than 500 m deep on 28 January. Strong sensible heat flux can enhance the ABL development in the morning. The ABL merged with the residual layer, and consequently the ABL depth increased abruptly at around 10 : 30 LT on 6 March, 11 : 30 LT on 24 April, and 09 : 30 LT on 31 May. On the other hand, the residual layer remained unchanged till 13 : 30 LT on 22 June, a day when rice seedlings were growing after irrigation. Much stronger echoes within the ABL on that day indicate turbulent structures associated with large humidity gradients. High humidity resulting from the strong water vapour flux over the surface affected the ABL structure. Daily maximum ABL depth occurred around 1500 m on 22 June and 3 July, even though the virtual sensible heat flux was smaller. Surface buoyancy flux does not explain such ABL development.

Figure 9 shows the daily maxima of the ABL depth and the virtual sensible heat flux averaged between 08 : 00 and 14 : 00 LT. There is a relationship between the ABL depth and the midday averaged heat flux before the field was irrigated, especially in winter. However, the relationship is less clear after irrigation. Also plotted in the figure is

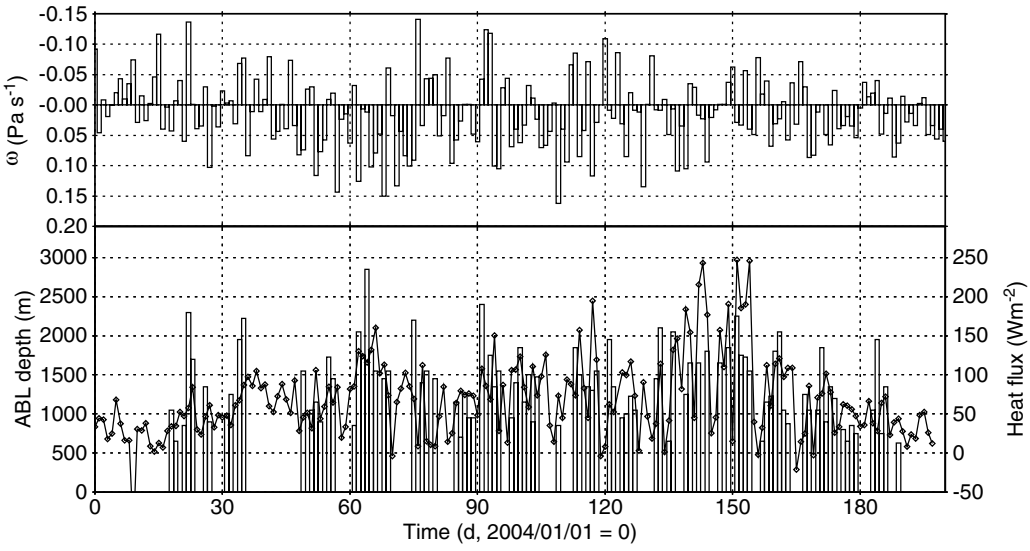

Figure 9. Seasonal changes in the observed daily maximum ABL height (bottom panel, bars), observed virtual sensible heat flux (bottom panel, rectangle with lines) between 08 : 00 and 16 : 00 LT, and the 925-hPa vertical pressure velocity (ω; upper panel, bars) extracted from the NCEP/NCAR re-analysis at 00Z (08 : 00 LT) at 32·5 °N, 117·5 °E. Negative ω indicates upward motion

DOI: 10.1002/hyp

the vertical pressure velocity ω at 925 hPa at 00Z (08 : 00 LT) at 32·5 °N and 117·5 °E from the National Center for Environmental Prediction (NCEP)/National Center for Atmospheric Research (NCAR) re-analysis (Kalnay *et al*., 1996), which represents an atmospheric vertical motion. The plotted vertical motion is near or slightly above the top of the ABL, which was usually close to or below 925 hPa at 08 : 00 LT. The vertical motion is representative of a $2{\cdot}5 \times 2{\cdot}5$-degree area between 31·25–33·75 °N and 116·25–118·75 °E, a region that includes the study site. Vertical motion can be linked to the discrepancies between the ABL depth and the heat flux, especially when the heat flux was low after irrigation.

Figure 10 shows the relationships between the daily ABL depth and the midday averaged virtual sensible heat flux for (a) the entire study, and for five periods including (b) winter (time = 0–59), (c) early spring (time = 60–89), (d) the growth period of wheat (time = 90–139), (e) the period with no vegetation after the wheat had been harvested and before irrigation (time = 140–164) and (f) after irrigation (time = 165–197). A

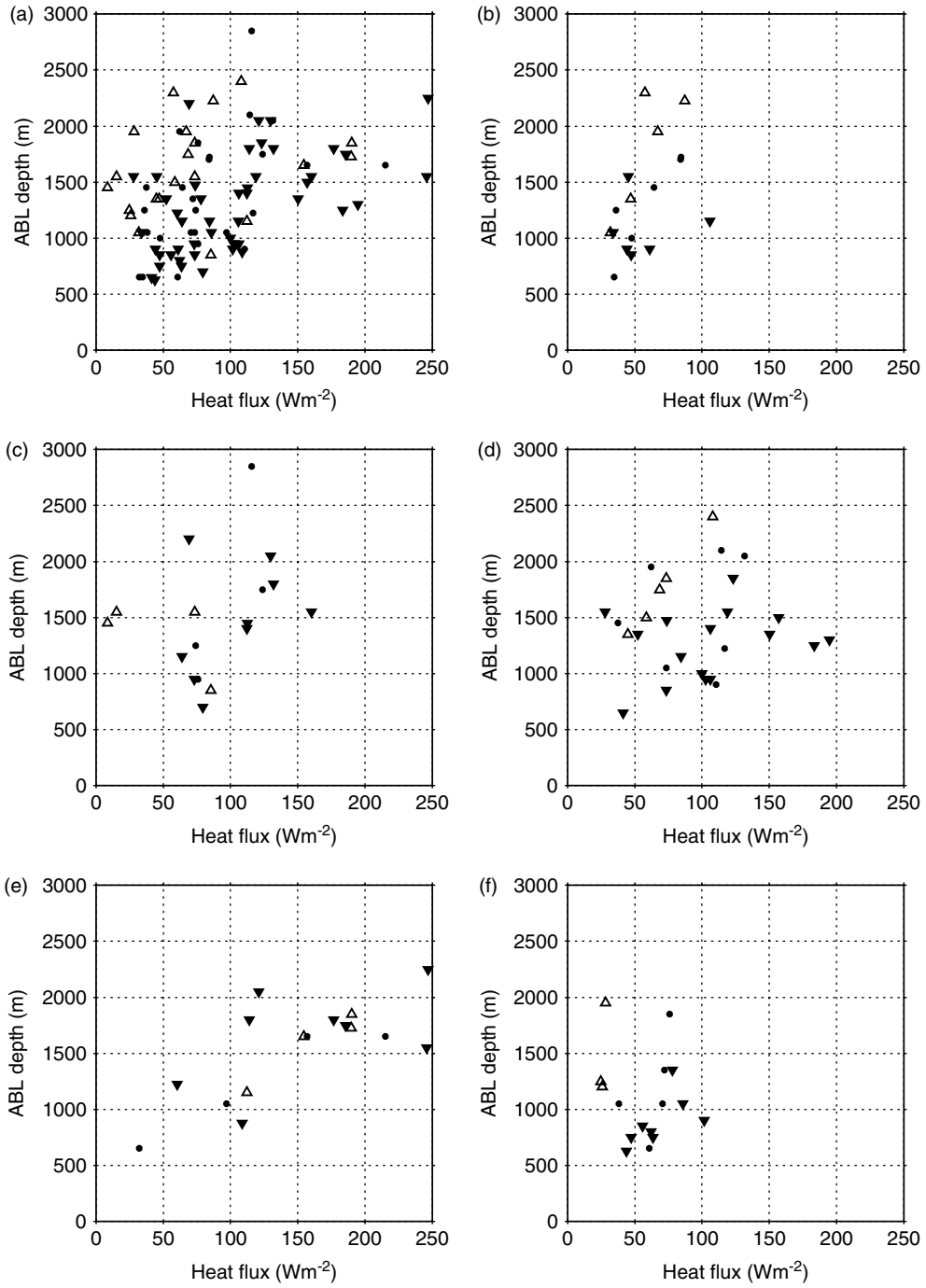

Figure 10. Relationships between the daily ABL depth and the midday averaged virtual sensible heat flux. Filled circles indicate neutral motion ($-0{\cdot}02 < \omega < 0{\cdot}02$), upward open triangles indicate ascending motion ($\omega < -0{\cdot}02$), and downward filled triangles indicate descending motion ($\omega > 0{\cdot}02$), where ω is the 925-hPa vertical pressure velocity from the NCEP/NCAR re-analysis, as shown in Figure 9

DOI: 10.1002/hyp

positive trend is evident in all periods except in period (f) after irrigation. The scatter in Figure 10 can be explained partly by atmospheric vertical motion after irrigation and in other periods except period (e). Downward motion suppressed the ABL development (downward triangles in Figure 10), whereas upward motion enhanced it (upward triangles in Figure 10). Other explanations for scatter may include residual layer effects and horizontal advection effects, which should be considered in future studies.

CONCLUDING REMARKS

The Surface and ABL observations in the LAPS project began in August 2003, and are ongoing. A preliminary analysis of the surface and ABL observations revealed relationships between the surface fluxes and the ABL structure. Buoyancy flux enhanced ABL development. Fluctuations in ABL depth were related to plume-like wind structures within the ABL. Daily variations in the ABL depth were controlled mainly by the buoyancy flux over the surface during the dry periods. Variations were strongly affected by atmospheric vertical motion during the wet periods, such as the Meiyu season. Further analysis to investigate how the ABL depth is affected by the combined effects of temperature and humidity profiles, in addition to surface fluxes, is warranted.

The source of the increased atmospheric humidity during the onset of Meiyu, and the mechanism that maintains humidity during the Meiyu season, may be the surface vapour flux caused by irrigation. Humid conditions affect the ABL structure and its development. In addition, synoptic-scale vapour transport may increase atmospheric humidity during the onset of Meiyu. Relationships between local phenomena and synoptic-scale humidity must be studied with further observations, satellite remote sensing, and re-analysis data such as NCEP/NCAR. Projections of water vapour transport at synoptic scales, i.e. weather forecasts, influence agricultural schedules. Interactions between anthropogenic hydrological activities and atmospheric phenomena also warrant future study.

ACKNOWLEDGEMENTS

This part of the Lower Atmosphere and Precipitation Study (LAPS) was conducted under the Core Research for Evolutional Science and Technology (CREST) program of the Japan Science and Technology Agency (JST) and the Hydrospheric Atmospheric Research Center (HyARC) at Nagoya University. The authors thank LAPS members for their cooperation and helpful discussions, CREST research manager Dr Shigeo Masuda for kind collaboration, and Ms Tomoko Tanaka for hard work with logistics. The authors thank Sumitomo Electronic Industries, Ltd., and Climatec, Inc. for the establishment of the observation systems. We also thank Shouxian Meteorological Observatory, Anhui Meteorological Bureau, and the China Meteorological Administration for their collaboration in this study.

REFERENCES

Angevine WM, White AB, Avery SK. 1994. Boundary layer depth and entrainment zone characterization with a boundary layer profiler. *Boundary-Layer Meteorology* **68**: 375–385.

Angevine WM, Baltink HK, Bosveld FC. 2001. Observations of the morning transition of the convective boundary layer. *Boundary-Layer Meteorology* **101**: 209–227.

Angevine WM, Grimsdell AW, Hartten LM, Delany AC. 1998. The Flatland boundary layer experiments. *Bulletin of the American Meteorological Society* **79**: 419–431.

Asanuma J, Dias NL, Kustas WP, Brutsaert W. 2000. Observations of neutral profiles of wind speed and specific humidity above a gently rolling land surface. *Journal of the Meteorological Society of Japan* **78**: 719–730.

Choi T, Hong J, Kim J, Lea H, Asanuma J, Ishikawa H, Tsukamoto O, Gao Z, Ma Y, Ueno K, Wang J, Koike T, Yasunari T. 2004. Turbulent exchange of heat, water vapor, and momentum over a Tibetan prairie by eddy covariance and flux variance measurements. *Journal of Geophysical Research-Atmospheres* **109**(D21): D21106.

Gao Z. 2005. Determination of soil heat flux in a Tibetan short-grass prairie. *Boundary-Layer Meteorology* **114**: 165–178.

Gao Z, Chae N, Kim J, Hong J, Choi T, Lee H. 2004. Modeling of surface energy partitioning, surface temperature and soil wetness in the Tibetan prairie using the Simple Biosphere Model 2 (SiB2). *Journal of Geophysical Research* **102**: D06102.

Garratt JR. 1992. *The Atmospheric Boundary Layer*. Cambridge University Press: New York; 316.

Hashiguchi H, Yamanaka MD, Tsuda T, Yamamoto M, Nakamura T, Adachi T, Fukao S, Sato T, Tobing DL. 1995. Diurnal variations of the planetary boundary layer observed with an L-band clear-air Doppler radar. *Boundary-Layer Meteorology* **74**: 419–424.

Hiyama T, Sugita M, Bergström H, Mölder M. 1999. Wind speed measurements in upper and lower boundary layers to determine regional momentum fluxes. *Agricultural and Forest Meteorology* **98–99**: 145–158.

Hiyama T, Strunin MA, Suzuki R, Asanuma J, Mezrin MY, Bezrukova NA, Ohata T. 2003. Aircraft observations of the atmospheric boundary layer over a heterogeneous surface in Eastern Siberia. *Hydrological Processes* **17**: 2885–2911.

Kalnay E, Kanamitsu M, Kistler R, Collins W, Deaven D, Gandin L, Iredell M, Saha S, White G, Woollen J, Zhu Y, Chelliah M, Ebisuzaki W, Higgins W, Janowiak J, Mo KC, Ropelewski C, Wang J, Leetmaa A, Rdynolds R, Jenne R, Joseph D. 1996. The NCEP/NCAR 40-year reanalysis project. *Bulletin of the American Meteorological Society* **77**: 437–471.

Kobayashi K, Abo T, Izumikawa Y, Kawahara K, Ishihara M, Wakayama T, Matsuda T. 2005. Development of a method of reducing the effect of echoes of migrating birds on wind measurements in the wind profiler network of JMA. *Bulletin Journal of the Meteorological Society of Japan, Tenki* **52**: 11–22, [in Japanese].

Komatsu H, Yoshida N, Takizawa H, Kosaka I, Tantasirin C, Suzuki M. 2003. Seasonal trend in the occurrence of nocturnal drainage flow on a forested slope under a tropical monsoon climate. *Boundary-Layer Meteorology* **106**: 573–592.

Ohta T, Suzuki K, Kodama Y, Kubota J, Kominami Y, Nakai Y. 1999. Characteristics of the heat balance above the canopies of evergreen and deciduous forests during the snowy season. *Hydrological Processes* **13**: 2382–2394.

Ohta T, Hiyama T, Tanaka H, Kuwada T, Maximov TC, Ohata T, Fukushima T. 2001. Seasonal variation in the energy and water exchanges above and below a larch forest in eastern Siberia. *Hydrological Processes* **15**: 1459–1476.

Reddy KK, Kozu T, Nakamura K, Ohno Y, Srinivasulu P, Anandan VK, Jain AR, Rao PB, Rao RR, Viswanthan G, Rao DN. 2001. Lower atmospheric wind profiler at Gadanki, tropical India: initial results. *Meteorologische Zeitschrift* **10**: 457–468.

Sellers PJ, Hall FG, Asrar G, Strebel DE, Murphy RE. 1992. An overview of the first international satellite land surface climatology project (ISLSCP) field experiment (FIFE). *Journal of Geophysical Research* **97**: 18345–18371.

Shinoda T, Uyeda H, Yoshimura K. 2005. Structure of moist layer and sources of water over the southern region far from the Meiyu/Baiu front. *Journal of the Meteorological Society of Japan* **83**: 137–152.

DOI: 10.1002/hyp

Sugita M, Endo N, Hiyama T. 1999. Regional surface momentum flux derived from atmospheric boundary layer bulk similarity approach. *Journal of Geophysical Research-Atmospheres* **104**(D14): 16965–16972.

Strunin MA, Hiyama T. 2004. Applying wavelet transforms to analyse aircraft-measured turbulence and turbulent fluxes in the atmospheric boundary layer over eastern Siberia. *Hydrological Processes* **18**: 3081–3098.

Strunin MA, Hiyama T, Asanuma J, Ohata T. 2004. Aircraft observations of the development of thermal internal boundary layers and scaling of the convective boundary layer over non-homogeneous land surfaces. *Boundary-Layer Meteorology* **111**: 491–522.

Tanaka K, Ishikawa H, Hayashi T, Tamagawa I, Ma Y. 2001. Surface energy budget at Amdo on the Tibetan plateau using GAME/Tibet IOP98 data. *Journal of the Meteorological Society of Japan* **79**: 505–517.

Tennekes HA. 1973. A model for the dynamics of the inversion above a convective boundary layer. *Journal of the Atmospheric Sciences* **30**: 558–567.

Toda M, Nishida K, Ohte N, Tani M, Musiake K. 2002. Observation of energy fluxes and evapotranspiration over terrestrial complex land-covers in the tropical monsoon environment. *Journal of the Meteorological Society of Japan* **80**: 465–484.

Wai M-K, Smith EA. 1998. Linking boundary layer circulations and surface processes during FIFE 89. Part II: maintenance of secondary circulation. *Journal of the Atmospheric Sciences* **55**: 1260–1276.

White AB, Templeman BD, Angevine WM, Zamora RJ, King CW, Russell CA, Banta RM, Brewer WA, Olszyna KJ. 2002. Regional contrast in morning transitions observed during the 1999 Southern Oxidants Study Nashville Middle Tennessee Intensive. *Journal of Geophysical Research-Atmospheres* **107**(D23): 4726.

Wilczak JM, Strauch RG, Ralph FM, Weber BL, Merritt DA, Jordan JR, Wolfe DE, Lewis LK, Wuertz DB, Gaynor JE. 1995. Contamination of wind profiler data by migrating birds: characteristics of corrupted data and potential solutions. *Journal of Atmospheric and Oceanic Technology* **12**: 449–467.

DOI: 10.1002/hyp